Journal of Photochemistry and Photobiology A: Chemistry 199 (2008) 322–329

Contents lists available at ScienceDirect

Journal of Photochemistry and Photobiology A: Chemistry

journal homepage: www.elsevier.com/locate/jphotochem

2,6-Diphenylpyridine-based organic emitter for electroluminescent device

Jin-Lin Zuo [a], Jia-Xiang Yang [a,c,*], Fu-Zhi Wang [b], Xiang-Nan Dang [b], Jian-Liang Sun [b], De-Chun Zou [b,**], Yu-Peng Tian [a,c], Na Lin [c], Xu-Tang Tao [c], Min-Hua Jiang [c]

[a] Department of Chemistry, Anhui University, Hefei 230039, PR China
[b] Key Laboratory of Polymer Chemistry & Physics of Education Ministry, Department of Polymer Science & Engineering, College of Chemistry and Molecular Engineering, Peking University, Beijing 100871, PR China
[c] State Key Laboratory of Crystal Materials, Shandong University, Jinan 250100, PR China

ARTICLE INFO

Article history:
Received 23 January 2008
Received in revised form 15 May 2008
Accepted 13 June 2008
Available online 26 June 2008

Keywords:
2,6-Diphenylpyridine-based
Organic emitter
Electroluminescent device
Photoluminescent
Fluorescence

ABSTRACT

2,6-Diphenylpyridine-based compound (**6**) was synthesized and fully characterized. The crystal structure of **6** was determined by single crystal X-ray diffraction determination. It is fluorescent in the blue–green region. The HOMO and LUMO energy levels obtained from electrochemical and UV–vis spectrum are −5.25 and −2.48 eV, respectively. INDO method in the ZINDO program was employed to study their electron density distribution. Using the dye as light-emitting layer without doping, organic light-emitting diodes showed appropriate green emission at λ_{max} = 518 nm. The device shows good performance with a low turn-on voltage of 3.10 V and a maximum brightness of 28,839 cd/m^2 at 14.71 V. The CIE coordinates calculated based on the EL data are (0.28, 0.58) close to the chromaticity coordinates of the NTSC standard green (x = 0.22, y = 0.71).

1. Introduction

Considerable progress has been made on organic light-emitting diodes (OLEDs) since the reports of Kodak's team [1] and Cambridge's group [2] on small molecule-based and polymer-based devices over a decade ago. OLEDs normally contain three layers, with hole-transporting, emitting and electron-transporting properties, respectively, sandwiched between suitable anodes and cathodes. When voltage is applied, the holes migrate through the hole-transporting material and loosely bond with the electrons at the interface with the electron-transporting layer (ETL) to form the excitons that are responsible for the emission of light [3]. Organic electroluminescent materials, which can offer fast responses, high brightnesses, low drive voltages, large areas, low production costs and ease of color tuning, have been extensively investigated for various full-color flat-panel display applications in recent years [4–7]. In order to realize full-color displays, red–green–blue materials with good color purity, sufficient brightness, high efficiency and adequate thermal stability are necessary [8]. The search for efficient and stable new emitting materials with proper CIE values for full-color displays remains as one of the most active areas of these studies. Among the well-known light-emitting materials, Alq_3 is considered as the most commonly used green host emitter. The Alq_3-based devices have been investigated in detail and have shown excellent properties in fabrication, lifetime and brightness [9,10]. In addition to Alq_3 and its derivatives [11,12], many green-light emitters have appeared in the literature [13–15]. Bis(10-hydroxybenzo[*h*]quinolinate) beryllium ($Bebq_2$) is known as an effective green-light host emitter [13]. Several carbazole derivatives have recently shown to be very efficient both as hole transporters and green emitters [14]. Pyridine-containing conjugated polymers have also been shown to be promising candidates for green light-emitting devices [16]. In this work, we wish to explain that by a proper choice of the hole-transporting, hole-blocker and electron-transporting materials, pyridine-derivative-based electroluminescent devices show high brightness and current efficiency, very low turn-on voltage and excellent CIE coordinates. 2,6-Diphenylpyridine-based compound was synthesized and fully characterized. The crystal structure of **6** was determined by single crystal X-ray diffraction determination. It was well soluble in most organic solvents. Its optical properties are also presented. Theoretical calculations have also been employed to study their electron density distribution. The physical data of the compound and the performance of the device are also illustrated [8].

* Corresponding author at: Department of Chemistry, Anhui University, Feixi Road No. 3, Hefei 230039, PR China. Tel.: +86 5515108151; fax: +86 5515107342.
** Corresponding author.
E-mail addresses: jxyang@ahu.edu.cn (J.-X. Yang), dczou@pku.edu.cn (D.-C. Zou).

1010-6030/$ – see front matter © 2008 Elsevier B.V. All rights reserved.
doi:10.1016/j.jphotochem.2008.06.013

2. Experimental

2.1. Materials and measurements

All commercially available chemicals were of analytical grade and used without further purification. In the experiment, the solvents were purified by conventional methods. IR spectra were recorded on NEXUS 870 (Nicolet) spectrophotometer in the 400–4000 cm^{-1} region using a powder sample on a KBr plate. The ^1H NMR and ^{13}C NMR spectra recorded on at 25 °C using Bruker Avance 400 spectrometer were reported as parts per million (ppm) from TMS (d). Coupling constants *J* were given in hertz. Mass spectrum was determined with a micromass GCT–MS (EI source). X-ray diffraction data of single crystals were collected on Bruker APEX2 CCD area-detector differactometer. The determination of unit cell parameters and data collections were performed with Mo Ka radiation (k = 0.71073 Å). Unit cell dimensions were obtained with least-squares refinements, and all structures were solved by direct methods using SHELXS-97. The other non-hydrogen atoms were located in successive difference Fourier syntheses. The final refinement was performed by full-matrix least-squares methods with anisotropic thermal parameters for non-hydrogen atoms on F2. The hydrogen atoms were added theoretically and riding on the concerned atoms. UV–vis absorption and emission spectra were recorded on UV-3600 spectrophotometer and Hitachi F-2500 fluorescence spectrometers, respectively. The single-photon-excited fluorescence quantum yields Φ were measured using a standard method under the same experimental conditions for title compound. Coumarin 307 dissolved in ethanol (Φ = 0.56) [17], at the same concentration as title compound, was used as the standard. Thermal gravimetric analysis (TGA) was carried out under a nitrogen atmosphere at a heating rate of 20 °C/min from 20 to 850 °C, with a Perkin-Elmer Diamond thermogravimetric analyzer. Cyclic voltammetry experiments were performed with a CHI630C electrochemical analyzer. All measurements were carried out at room temperature with a conventional three-electrode configuration consisting of a platinum working electrode, an auxiliary platinum electrode and a non-aqueous Ag/AgCl reference electrode. The solvent in this experiment was dichloromethane, and the supporting electrolyte was tetra-*n*-butylammonium perchlorate (TBAP). The onset potentials were determined from the intersection of two tangents drawn at the rising current and background current of the cyclic voltammogram. According to the oxidation onset potentials of the CV measurements, the HOMO energy level of the material is estimated based on the reference energy level of normal hydrogen electrode (NHE) (4.50 eV below the vacuum): HOMO = $-(E_{onset} + 0.20\,V) - 4.50\,eV$, where the value 0.20 V is for Ag/AgCl vs NHE [18].

2.2. Synthesis of 1-phenyl-3-p-tolyl-2-alkene-1-ketone **1** [19]

A flask was charged with a mixture of *p*-toluadehyde (6.00 g, 50 mmol), acetophenone (6.00 g, 50 mmol) and 2% aqueous sodium hydroxide (150 mL), and the mixture was vigorously stirred at room temperature for 30 min, then heated about 60 °C for 6 h. The reaction was monitored by TLC. After the reaction, a light yellow solid was filtered, washed with water and air-dried to give 10.90 g. Yield: 98.20%. IR (cm^{-1}): 3049, 1655, 1599, 1334, 982, 690. ^1H NMR ($CDCl_3$, 400 MHz, ppm) δ: 2.39 (s, 3H), 7.23 (d, 2H, J = 8.00 Hz), 7.47–7.60 (overlapping multiples, 6H), 7.80 (d, 1H, J = 15.70 Hz), 8.00–8.04 (m, 2H). ^{13}C NMR ($CDCl_3$, 100.61 MHz, ppm) δ: 21.05, 120.67, 127.96–128.20 (m), 129.24, 131.71, 132.17, 137.92, 140.60, 144.45, 190.15.

2.3. Synthesis of 1,5-diphenyl-3-p-tolyl-1,5-dione **2** [19]

Acetophenone (2.40 g, 20 mmol), 1-phenyl-3-*p*-tolyl-2-alkene-1-ketone **1** (4.40 g, 20 mmol) and powder NaOH (3.20 g, 80 mmol) were crashed together with a pestle and mortar for 2 h to give the residue, which was recrystallized from ethanol to give white needle crystal. Yield: 6.20 g, 90.60%. IR (cm^{-1}): 2914, 1674, 1595, 1238, 978, 687. ^1H NMR ($CDCl_3$, 400 MHz, ppm) δ: 2.28 (s, 3H), 3.40 (m, 4H), 4.02 (m, 1H), 7.08 (d, 2H, J = 7.90 Hz), 7.16 (d, 2H, J = 7.90 Hz), 7.43 (t, 4H), 7.53 (m, 2H), 7.90–7.96 (m, 4H). ^{13}C NMR ($CDCl_3$, 100.61 MHz, ppm) δ: 20.53, 36.39, 44.57, 126.82, 127.68, 128.09, 128.80, 132.54, 135.75, 136.49, 140.30, 198.18.

2.4. Synthesis of 4-p-tolyl-2,6-diphenylpyridine **3** [19]

1,5-Diphenyl-3-*p*-tolyl-1,5-dione **2** (3.40 g, 10 mmol) was added to a stirred solution of ammonium acetate (8 g, excess) in ethanol (100 mL). The reaction mixture was heated at reflux for 10 h. Upon cooling to room temperature, a precipitate was filtered, washed with water three times and dried to afford the product, purified by flash column chromatography on silica. Elution with petroleum:ethyl acetate (8:1) gave a white solid. Yield: 1.90 g, 59.40%. IR (cm^{-1}): 3034, 1599, 1387, 1026, 814, 687. ^1H NMR ($CDCl_3$, 400 MHz, ppm) δ: 2.46 (s, 3H), 7.35 (d, 2H, J = 8.02 Hz), 7.40–7.60 (m, 6H), 7.67 (d, 2H, J = 8.02 Hz), 7.90 (s, 2H), 8.22 (d, 4H, J = 8.02 Hz). ^{13}C NMR ($CDCl_3$, 100.61 MHz, ppm) δ: 20.79, 116.47, 126.54, 126.71, 128.22, 128.55, 129.38, 135.61, 138.65, 139.14, 149.66, 156.98

2.5. Synthesis of 4′-(phenyl-p-bromomethyl)-2,6-diphenylpyridine **4** [19]

4-*p*-Tolyl-2,6-diphenylpyridine **3** (6.42 g, 20 mmol), NBS (4 g, 22 mmol) and a catalytic amount of benzoyl peroxide (BPO, 0.16 g) were mixed in tetrachloromethane (150 mL). The mixture was refluxed for 12 h. The reaction was monitored by TLC (petroleum:ethyl acetate, 4:1). After the reaction was completed, the mixture was dispersed in 100 mL water. The solution was extracted with CH_2Cl_2 three times. The organic layer was washed with water and saturated brine consequently. The organic extracts were dried over $MgSO_4$. The solvent was removed in vacuo, and the residue was transferred to the top of a silica gel chromatography column which was eluted with petroleum:ethyl acetate (8:1) gave a white solid. Yield: 7 g, 87.50%. ^1H NMR ($CDCl_3$, 400 MHz, ppm) δ: 4.58 (s, 2H), 7.55 (m, 10H), 7.74 (d, 2H, J = 8.20 Hz), 7.88 (s, 2H), 8.20 (m, 2H). ^{13}C NMR ($CDCl_3$, 100.61 MHz, ppm) δ: 32.31, 45.24, 116.00, 126.68, 127.13, 128.25, 128.67, 128.87, 129.33, 138.44, 149.04, 157.12.

2.6. Synthesis of compound 4-(2,6-diphenylpyridine-4′)-benzyl triphenyl phosphonium bromide **5** [20]

4′-(Phenyl-*p*-bromomethyl)-2,6-diphenylpyridine **4** (5.74 g, 14 mmol) and trimethyl phosphate (3.77 g, 14 mmol) were mixed in dried benzene (150 mL). The mixture was refluxed for 12 h. After the reaction was completed, the solvent was removed under reduced pressure, and cooled to room temperature. After addition of ethanol, the mixture was vigorously stirred at room temperature for 30 min. A white solid precipitate was filtered, washed with ethanol and air-dried to give 7.53 g. Yield: 79.20%. The product participated in the next reaction without being characterized.

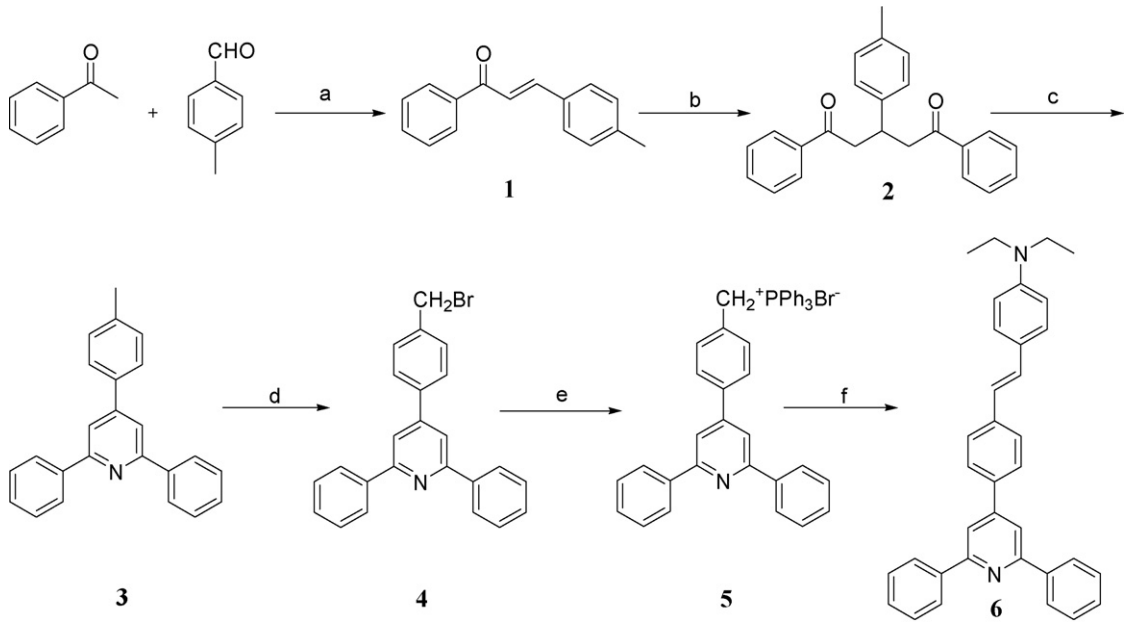

Scheme 1. Synthesis of **6**: (a) 2% aqueous sodium hydroxide, reflux; (b) acetophenone, NaOH; (c) CH_3COONH_4, ethanol, reflux; (d) NBS, BPO, CCl_4, reflux; (e) PPh_3, benzene, reflux; (f) 4-diethylaminobenzaldehyde, *t*-BuOK, grind.

*2.7. Synthesis of compound 4′-(4-{2-[4-(diethylamino)phenyl]ethenyl}phenyl)-2,6-diphenylpyridine **6** (Scheme 1)*

Fresh *t*-BuOK (672 mg, 6.00 mmol) was placed in a dry mortar and milled to very small, then compound 4-(2,6-diphenylpyridine-4′)-benzyl triphenyl phosphonium bromide **5** (661.20 mg, 1.00 mmol) and 4-diethylaminobenzaldehyde (200 mg, 1.13 mmol) were added and mixed equably. The mixture was milled vigorously for about 20 min, and became sticky. After completion of the reaction (the reaction was monitored by TLC; petroleum:ethyl acetate, 4:1), the mixture was dispersed in 100 mL water. The solution was extracted with CH_2Cl_2 three times. The organic layer was washed with water and saturated brine consequently. The organic extracts were dried over $MgSO_4$. The solvent was removed in vacuo, the residue was transferred to the top of a silica gel chromatography column which was eluted with petroleum:ethyl acetate (8:1). The strong green fluorescence was collected, and 252 mg product **6** was obtained with 52.50% yield. IR (KBr, cm^{-1}): 2924, 1595, 1439, 1188, 692. ^1H NMR ($CDCl_3$, 400 MHz, ppm) δ: 1.08 (m, 6H), 3.35 (m, 4H), 6.67 (d, 2H, J = 8.40 Hz), 7.02 (d, 1H, J = 16.00 Hz), 7.24 (d, 1H, J = 16.40 Hz), 7.47 (m, 4H), 7.56 (t, 4H), 7.70 (d, 2H, J = 8.00 Hz), 8.03 (d, 2H, J = 8.00 Hz), 8.16 (d, 2H, J = 26.00 Hz), 8.33 (d, 4H, J = 7.60 Hz). ^{13}C NMR ($CDCl_3$, 100.61 MHz, ppm) δ: 12.95, 18.90, 44.15, 111.92, 116.46, 122.56, 126.83, 127.40, 127.97, 128.58, 129.22, 129.68, 130.41, 135.70, 139.33, 139.65, 149.55, 157.01. MS (EI), *m/z*: 480 (M^+), 465 (M^+-CH_3).

2.8. Devices fabrication and characterization

Four-layer devices were fabricated with a configuration of indium tin oxide ITO/NPB (30 nm)/**6** (40 nm)/BCP (10 nm)/Alq_3 (20 nm)/Mg:Ag (10:1, mass ratio, 150 nm)/Ag (10 nm), in which 4,4′-bis[*N*-(1-naphthyl)-*N*-phenylamino]biphenyl (NPB) as hole-transport layer, **6** as the emitting layer, 2,9-dimethyl-4,7-diphenyl-1,10-phenanthroline (BCP) as a hole-blocker layer, tris(8-hydroxyquinoline)aluminum (Alq_3) as electron transport layer. The ITO glass was cleaned in ultrasonic baths of detergent, deionized water and acetone in sequence, and followed oxygen plasma cleaning. The organic films and metal electrode were sequentially deposited on the substrate by thermal evaporation under a vacuum of 10^{-6} Torr. The deposition rates were 2–3 Å/s for the organic materials and 5–7 Å/s for the cathode metals. The emitting area of the device was 4 mm^2. The thickness of films was measured by a Dektak surface profilometer. The EL spectra and current–voltage–luminance (J–V–L) characteristics were measured with a Spectra scan PR 650 photometer and a computer-controlled DC power supply. All the measurements of the devices were carried out under ambient conditions.

3. Results and discussion

3.1. Structure features

The crystal of **6**, suitable for the X-ray analysis, was obtained from slow evaporation CH_2Cl_2 covered with ethanol at room temperature several days later (Table 1). The selected bond distances and angles are listed in Table 2. As shown in Fig. 1, it is obvious

Table 1
Crystal data collection and structure refinement of **6**

Molecule	**6**
Formula	$C_{35}H_{32}N_2$
Formula weight	480
Crystal system	Orthorhombic
Space group	*Pca*2(1)
Temperature (K)	293(2)
λ of Mo Ka (Å)	0.71069
Absorption coefficient (mm^{-1})	0.093
a (Å)	9.981(5)
b (Å)	13.461(5)
c (Å)	41.256(5)
α (°)	90.000(5)
β (°)	90.000(5)
γ (°)	90.000(5)
V ($Å^3$)	5543(4)
Z	4
Reflections collected	10950
Reflections unique	4024
Final *R* indices	$[I > 2r(I)]R_1 = 0.0698$, $wR_2 = 0.1274$

Table 2
Selected bond lengths (Å) and angles (°) of **6**

C8–C11	1.450
C12–C13	1.456
C4–N1	1.445
C2–N1–C4	116.09
C4–N1–C5	120.45
C11=C12	1.312
C2–N1	1.436
C5–N1	1.375
C2–N1–C5	120.83

that the C=C exists in trans-isomer, making for planar construction of molecular. In the diphenylpyridine acceptor moiety, the central pyridinyl (labeled P0) is also arranged with three phenyl planes (P1, P2 and P3) being 6.53° (between P0 and P1), 13.10° (P0 and P2) and 13.10° (P0 and P3). The result indicates that the diphenylpyridine group is seldom coplanar. At the diethylamino donor end, the central nitrogen and its three bended carbon atoms are basically coplanar, forming a quasi-equilateral trigonal NC3 plane (defined as the P5 plane), with the sum of the three C–N–C angles (357.37°) being close to 360°. In fact, the entire aniline groups are basically coplanar. This coplanarity of the trigonal NC_3 in chromophore **6** implies that the lone pair of the electrons may be highly delocalized into the large π-system, even in the ground state. The linkage between two phenyl rings (P1 and P4) is quite conjugated with bond lengths of C8–C11: 1.450 Å, C11 = C12: 1.312 Å and C12–C13: 1.456 Å. These structural features suggest that all non-hydrogen atoms between donor and acceptor are highly conjugated, leading to a π-bridge for the charge transfer from the central diethylamino moiety to the phenylpyridine unit.

3.2. Photophysical properties

The optical properties of the **6** were measured both in solution and in thin film, and the corresponding spectra were shown in Fig. 2. The concentration of the solution for the measurements of UV–vis and photoluminescent (PL) spectra was 1.00×10^{-5} and 1.00×10^{-6} M in benzene, respectively. The thin film for UV–vis and PL measurements was prepared by spin-coating from dichloromethane solution on a quartz plate followed by drying for 2 h at room temperature. The optical properties data for **6** were summarized in Table 3. As shown in Fig. 2, the solution and the film show absorption maximum at 382 and 396 nm, respectively, which correspond to the π–π* transition of the main chain [21]. Note that the absorption profiles and the absorption maxima are mainly dominated by the nature of the excited state π-electron system [20,22]. The band gap energy figured out from the UV–vis spectrum of **6** film is 2.77 eV. The solution and the film emit blue–green light with a maximum at 482 and 497 nm, respectively. The emitting wavelength of **6** shows more significantly red shifts in the solid film than those in solution, which implies that there are stronger interactions among dye than between solvent and dye. Therefore, this material has probably strong fluorescence quenching in the solid film [23]. Note that the emission profiles and the emission maxima mainly reflect the nature of the ground state π-electron system [20,22]. Using coumarin 307 as a reference, fluorescence quantum

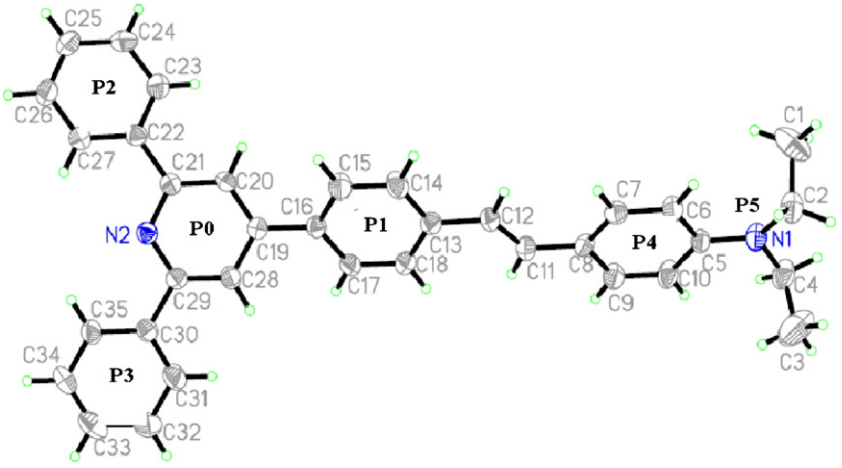

Fig. 1. Crystal structure of **6**.

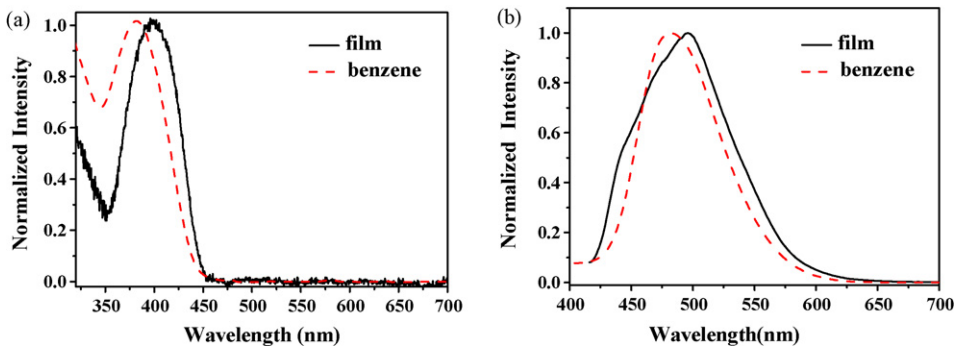

Fig. 2. (a) Solution and film absorption spectra of **6** and (b) solution and film emission spectra of **6**.

Table 3
Summary of the optical and electrochemical properties data for **6**

Compound	λ_{ab}^{max} (nm)		λ_{em}^{max} (nm)		E_g^{opt} (eV)[a]	E_{onset}^{ox} (V)[b]	HOMO (eV)[c]	LUMO (eV)[d]
	Solution[e]	Film	Solution[e]	Film				
6	382	396	482	497	2.77	0.55	−5.25	−2.48

[a] Optical band gap, calculated from the absorption edge of the UV–vis spectrum.
[b] Potential values are listed vs Ag/AgCl.
[c] Determined from the onset oxidation potential, HOMO = $-(E_{onset} + 0.20\,V) - 4.50\,eV$, where the value 0.20 V is for Ag/AgCl vs NHE.
[d] $E_{LUMO} = E_{HOMO} + E_g$.
[e] The concentration of the solution for the measurements of UV–vis and photoluminescent (PL) spectra was 1.00×10^{-5} and 1.00×10^{-6} M in benzene, respectively.

yield (Φ) of **6** was obtained. Compound **6** shows a moderately high fluorescence quantum yield with $\Phi = 0.67$. In order to examine the potential application of the new synthesized compound, **6** selected as the candidate for electroluminescent (EL) device fabrication due to its higher solubility and easier fabrication. Therefore, thermal properties, electrochemistry and electroluminescence studies of **6** were carried out.

3.3. Thermal stability

To study the thermal stability of the title compound, TGA was performed on the single crystal sample in the range 20–850 °C (Fig. 3). The title compound is stable up to 269.2 °C and then keeps losing weight from 269.2 to 840.5 °C, indicating that it possess good thermal stability.

3.4. Electrochemical properties

In the device to fabricate and investigate the OLED characteristics of **6**, information on the electronic structure of the luminescent compound is essential. Cyclic voltammetry was used to investigate the redox behavior of the compound and to assess the HOMO and LUMO energy levels [21,24]. The electrochemical properties data for **6** were summarized in Table 3. The cyclic voltammogram for the selected compound is shown in Fig. 4. The couple of reversible oxidation process is probably attributed to the removal of one electron from the diethylamino unit [23]. Moreover, the reversible nature of these peaks indicates the electrochemical stability of the compound [25]. The energy gap was determined by the absorption edge of the absorption spectra (2.77 eV) of the sample films on quartz substrates [23]. The HOMO energy level vs vacuum level was calculated from the measured onset potential of oxidation (0.55 V vs Ag/AgCl) (Fig. 4) by assuming that the energy level of NHE is 4.50 eV below the vacuum level, and the LUMO energy level was calculated from the HOMO energy level and the absorption edge. The HOMO and LUMO energy levels obtained from electrochemical and UV–vis spectrum are −5.25 and −2.48 eV, respectively. Thus, the charge-trapping mechanism will play an important role in improving the device efficiency. The higher electron affinity of **6** could also decrease the energy barrier for electron injection. LUMO levels of the compound (6: 2.48 eV) in a neat solid were low enough to easily accept electrons from a cathode metal such as Mg:Ag (work function: 3.7 eV). This nature was caused by the electron-accepting moiety (pyridine) [26].

3.5. Quantum chemical calculations [23]

To understand the energy levels and to get further information about the charge-transferring electronic structure of the dye, quantum chemical calculations are performed with INDO method in the ZINDO program. The optimal molecular orbitals of the ground state for the dyes are shown in Fig. 5. In the HOMO, the electrons are mainly concentrated on the nitrogen atom of the diethylamino and its adjacent ethenylbenzene unit. In the LUMO, the electrons spread over the molecule along the molecular axis. Obviously, the electron transition from the HOMO to the LUMO is accompanied by charge transfer from the central diethylamino moiety to the phenylpyridine unit.

3.6. Electroluminescent properties

With indium tin oxide (ITO) as the anode, 30 nm of 4,4′-bis[*N*-(1-naphthyl)-*N*-phenylamino]biphenyl (NPB) as hole-transport layer, 40 nm of **6** as the emitting layer, 10 nm of 2,9-dimethyl-4,7-diphenyl-1,10-phenanthroline (BCP) as a hole-blocker layer, 20 nm of tris(8-hydroxyquinoline)aluminum (Alq_3) as electron transport layer. An alloy of magnesium and silver (10:1, mass ratio, 150 nm) as the cathode, which was capped with 10 nm of silver, devices with structure of ITO/NPB (30 nm)/**6** (40 nm)/BCP (10 nm)/Alq_3 (20 nm)/Mg:Ag (10:1, mass ratio, 150 nm)/Ag (10 nm) was fabricated by thermal vacuum deposition. The device

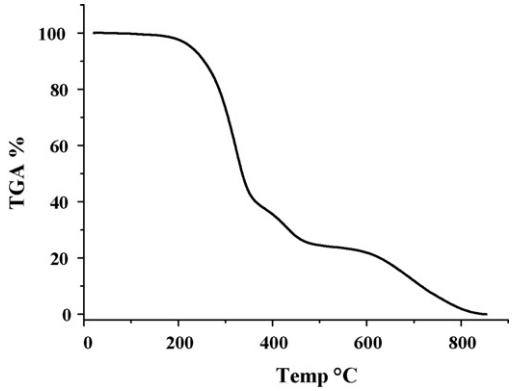

Fig. 3. The TGA diagram of **6**.

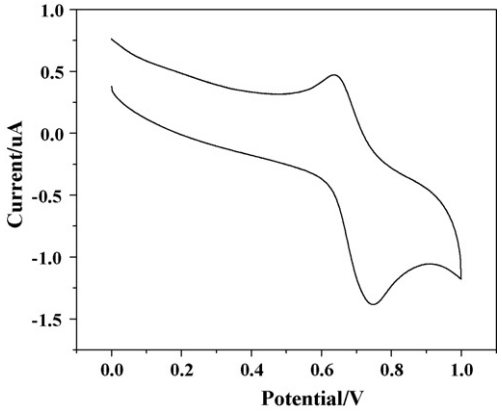

Fig. 4. Cyclic voltammetry (CV) of **6**.

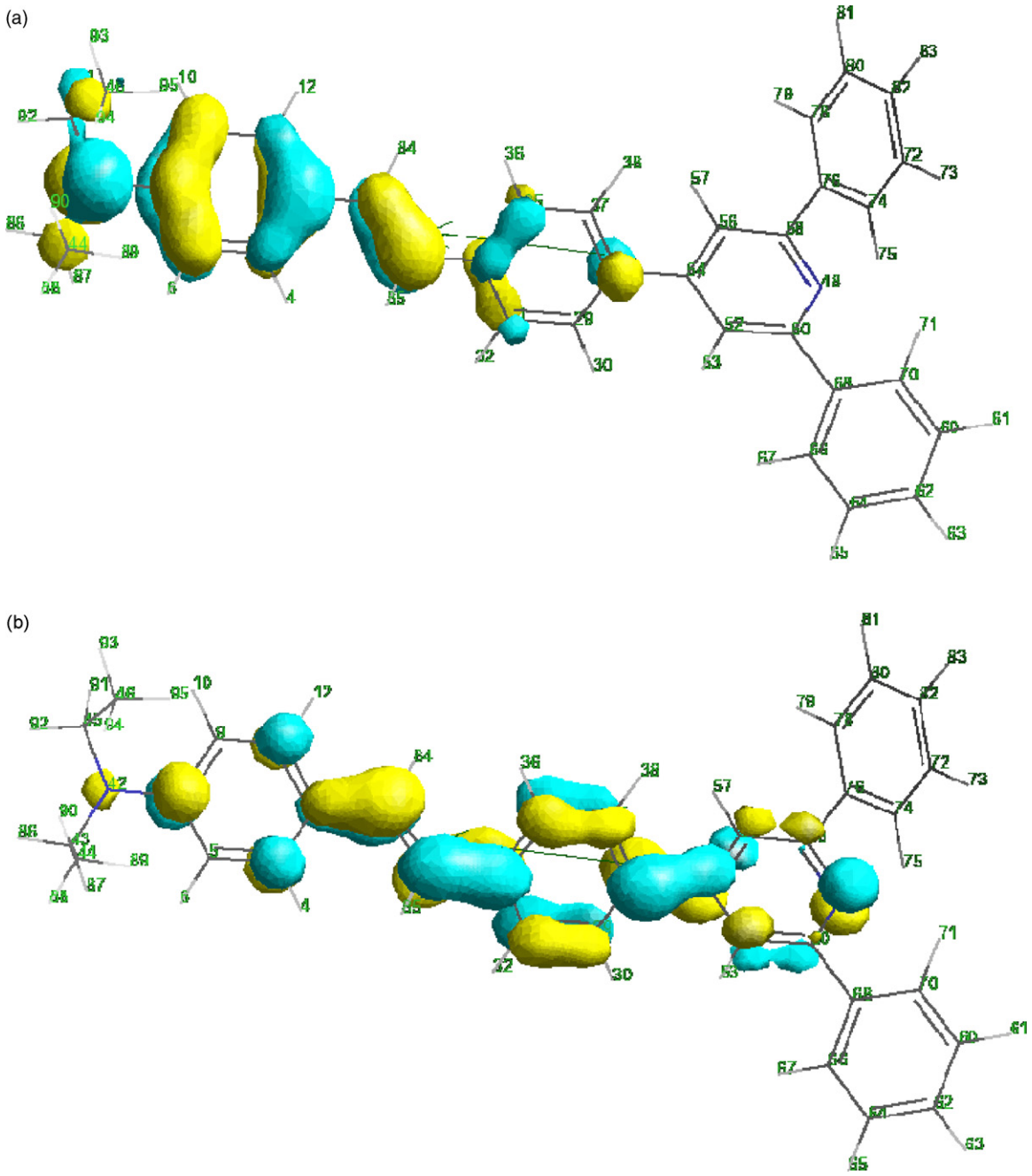

Fig. 5. Energy level and electron density distribution of frontier molecular orbital: (a) **6**—HOMO and (b) **6**—LUMO.

performances are summarized in Table 4. There is essentially no change in the EL spectrum (Fig. 6) between 4 and 14 V. The material showed appropriate green emission at λ_{max} = 518 nm. Fig. 7 shows the current–voltage–luminance characteristics of the OLEDs. The device based on **6** shows good performance with a low turn-on voltage of 3.10 V and a maximum brightness of 28,839 cd/m^2 at 14.71 V. Fig. 8 illustrates the current efficiency–power efficiency–current density characteristics of the device. A maximum current efficiency of 2.63 cd/A was obtained at a current density of 2.57 mA/cm^2. The device showed a gradual decreasing in current efficiency (η_I) with increasing current density. However, it remained high η_I of 2.23 cd/A at the high current density of 500 mA/cm^2. Although its efficiency is not too high, it can be further improved by optimizing the device structure. The CIE coordinate calculated based on the EL data is (0.28, 0.58) close to the chromaticity coordinate of the NTSC standard green (x = 0.22, y = 0.71) [8]. The EL spectrum of

Table 4
Summary of device performance data for **6**

U_{oneset} (V)	L_{max} (cd/m^2)	$\eta_{L_{max}}$ (lm/W)	$\eta_{I_{max}}$ (cd/A)	CIE coordinate (8 V)	λ_{max} (nm) (low voltage)
3.10	28,839	1.65	2.63	(0.28, 0.58)	518

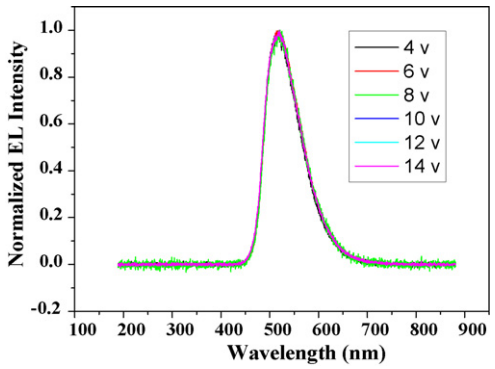

Fig. 6. EL spectra of **6** from ITO/NPB/**6**/BCP/Alq_3/Mg:Ag/Ag run at 4–14 V.

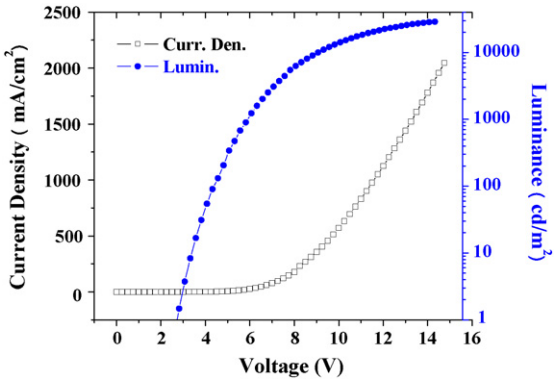

Fig. 7. Current density–voltage–brightness characteristics of devices of ITO/NPB/**6**/BCP/Alq_3/Mg:Ag/Ag.

6 closely resembles the PL spectrum, particularly in the half-bandwidth and the lowest and highest emission edges of the spectrum (Figs. 2 and 6). Although Alq_3 also reveals a maximum emission at the wavelength very close to the value of **6**, we can conclude that the excitons are confined in the **6** layer through the HOMO and LUMO energy levels of layers for the device ITO/NPB (30 nm)/**6** (40 nm)/BCP (10 nm)/Alq_3 (20 nm)/Mg:Ag (10:1, mass ratio, 150 nm)/Ag (10 nm). Analysis of the HOMO and LUMO energy levels of layers for this device was shown in Fig. 9. HOMO energy level of **6** (5.25 eV) lies between those of NPB (5.23 eV) and that of BCP (6.70 eV) [27], whereas the LUMO energy level of

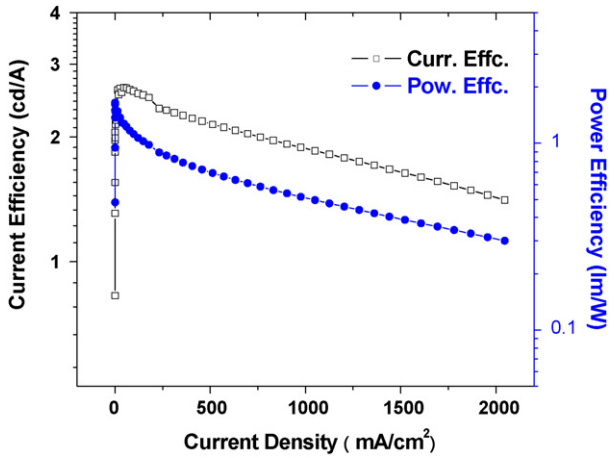

Fig. 8. Current efficiency–power efficiency–current density characteristics of devices of ITO/NPB/**6**/BCP/Alq_3/Mg:Ag/Ag.

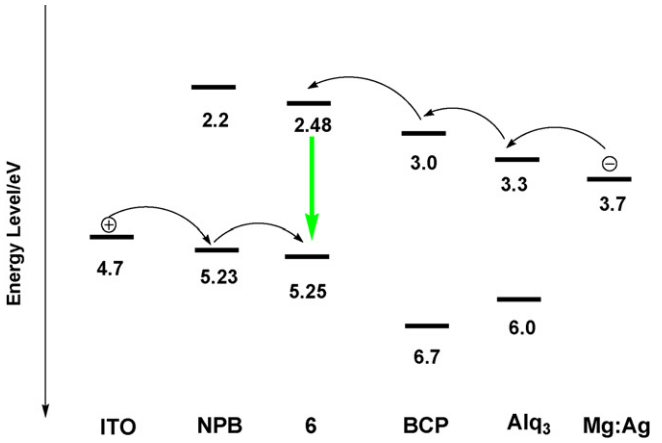

Fig. 9. Relative HOMO/LUMO energy levels of device ITO/NPB/**6**/BCP/Alq_3 /Mg:Ag/Ag.

6 (2.48 eV) lies between those of BCP (3.20 eV) and that of NPB (2.20 eV). There is a barrier of 1.45 eV for holes to migrate from **6** to BCP layer. Thus, under the present configuration [ITO/NPB (30 nm)/**6** (40 nm)/BCP (10 nm)/Alq_3 (20 nm)/Mg:Ag (10:1, mass ratio, 150 nm)/Ag (10 nm)], BCP acts as a hole blocker and the charge recombination is confined to **6** layer. The observations strongly indicate that the **6** instead of Alq_3 layer is responsible for the emission of the green light. These results are in contrast to a vast number of electroluminescent devices using arylamines as the hole-transport materials and Alq_3 as the electron-transport material [1,28]. In these devices, light generally emits from the Alq_3 layer due in part to the fact that hole mobility in the arylamine layer is faster than the electron migration in Alq_3 by a magnitude of a few orders and holes and electrons recombine in the Alq_3 layer [8,29].

4. Conclusions

In summary, we have presented the synthesis, characterization and crystal structure of a novel phenylpyridine derivative prepared from a solvent-free reaction. Its photoluminescence properties were studied. It had saturated blue–green emission, moderately high fluorescence intensity and chemical stability. The HOMO and LUMO energy levels obtained from electrochemical and UV–vis spectrum are −5.25 and −2.48 eV, respectively. The electron transition from the HOMO to the LUMO is accompanied by charge transfer from the central diethylamino moiety to the phenylpyridine unit. EL device with green emission was fabricated. We can conclude that the excitons are confined in the **6** layer through the HOMO and LUMO energy levels of layers for the device ITO/NPB (30 nm)/**6** (40 nm)/BCP (10 nm)/Alq_3 (20 nm)/Mg:Ag (10:1, mass ratio, 150 nm)/Ag (10 nm). Maximum luminance reached 28,839 cd/m^2 and the maximum power efficiency was 1.65 lm/W.

Acknowledgments

This work was supported by grants from the National Natural Science Foundation of China (50532030, 50673003), 973 programs of the People's Republic of China (90401028), Doctoral Program Foundation of the Ministry of Education of China, Education Committee of Anhui Province (2006KJ032A, 2006KJ135B), the National Natural Science Foundation of Anhui Province (070414188), the Key Project of Chinese Ministry of Education (06060347), Team for Scientific Innovation Foundation of Anhui Province (2006KJ007TD), and the Ministry of Education and Person with Ability Foundation of Anhui University.

References

[1] C.W. Tang, S.A. Van Slyke, Appl. Phys. Lett. 51 (1987) 913–915.
[2] J.H. Burroughes, D.D.C. Bradley, A.R. Brown, R.N. Marks, K. Mackay, R.H. Friend, P.L. Burn, Nature 347 (1990) 539–541.
[3] K.R.J. Thomas, J.T. Lin, Y.T. Tao, C.H. Chuen, Chem. Mater. 14 (2002) 2796–2802.
[4] C.C. Kwok, M.S. Wong, Chem. Mater. 14 (2002) 3158–3166.
[5] A. Kraft, A.C. Grimsdale, A.B. Holmes, Angew. Chem. Int. Ed. Engl. 37 (1998) 402–428.
[6] R.H. Friend, R.W. Gymer, A.B. Holmes, J.H. Burroughes, R.N. Marks, C. Taliani, D.D.C. Bradley, D.A. Dos Santos, J.L. Brédas, M. Lögdlund, W.R. Salaneck, Nature 397 (1999) 121–128.
[7] U. Mitschke, P. Bäuerle, J. Mater. Chem. 10 (2000) 1471–1507.
[8] M.X. Yu, J.P.C. Duan, H. Lin, C.H. Cheng, Y.T. Tao, Chem. Mater. 14 (2002) 3958–3963.
[9] M. Uekawa, Y. Miyamoto, H. Ikeda, K. Kaifu, T. Ichi, T. Nakaya, Thin Solid Films 352 (1999) 185–188.
[10] C.C. Tong, K.C. Hwang, J. Phys. Chem. C 111 (2007) 3490–3494.
[11] J. Kido, Y. Iizumi, Chem. Lett. 26 (1997) 963–964.
[12] L.S. Sapochak, A. Padmaperuma, N. Washton, F. Endrino, G.T. Schmett, J. Marshall, D. Fogarty, P.E. Burrows, S.R. Förrest, J. Am. Chem. Soc. 123 (2001) 6300–6307.
[13] Y. Hamada, T. Sano, M. Fujita, T. Fujii, Y. Nishio, K. Shibata, Chem. Lett. 22 (1993) 905–906.
[14] K.R.J. Thomas, J.T. Lin, Y.T. Tao, C.W. Ko, J. Am. Chem. Soc. 123 (2001) 9404–9411.
[15] L.L. Wu, S.H. Tsai, T.F. Guo, C.H. Yang, I.W. Sun, J. Lumin. 126 (2007) 687–694.
[16] Y.Z. Wang, A.J. Epstein, Acc. Chem. Res. 32 (1999) 217–224.
[17] G.A. Reynolds, K.H. Drexhage, Opt. Commun. 13 (1975) 222.
[18] M.S. Liu, J.D. Luo, A.K. Jen, Chem. Mater. 15 (2003) 3496–3500.
[19] J.X. Yang, X.T. Tao, C.X. Yuan, Y.X. Yan, L. Wang, Z. Liu, Y. Ren, M.H. Jiang, J. Am. Chem. Soc. 127 (2005) 3278–3279.
[20] Z.J. Hu, J.X. Yang, Y.P. Tian, H.P. Zhou, X.T. Tao, G.B. Xu, W.T. Yu, X.Q. Yu, M.H. Jiang, J. Mol. Struct. 839 (2007) 50–57.
[21] J.H. Kim, H. Lee, Chem. Mater. 14 (2002) 2270–2275.
[22] B. Valeur, Molecular Fluorescence—Principles and Applications, Wiley, Weinhaim, 2002.
[23] H.D. Ju, X.T. Tao, Y. Wan, J.H. Shi, J.X. Yang, Q. Xin, D.C. Zou, M.H. Jiang, Chem. Phys. Lett. 432 (2006) 321–325.
[24] Z. Peng, M.E. Galvin, Chem. Mater. 10 (1998) 1785–1788.
[25] C.W. Chiu, T.J. Chow, C.H. Chuen, H.M. Lin, Y.T. Tao, Chem. Mater. 15 (2003) 4527–4532.
[26] M. Ichikawa, T. Kawaguchi, K. Kobayashi, T. Miki, K. Furukawa, T. Koyama, Y. Taniguchi, J. Mater. Chem. 16 (2006) 221–225.
[27] Z. Gao, C.S. Lee, I. Bello, S.T. Lee, R.M. Chen, T.Y. Luh, J. Shi, C.W. Tang, Appl. Phys. Lett. 74 (1999) 865–867.
[28] K.R.J. Thomas, J.T. Lin, Y.T. Tao, C.W. Ko, Chem. Mater. 14 (2002) 1354–1361.
[29] C. Hosokawa, H. Tokailin, H. Higashi, T. Kusumoto, Appl. Phys. Lett. 60 (1992) 1220–1222.